

Dynamics of coupled modified Rössler oscillators: the role of nonisochronicity parameter

C. Ramya,¹ R. Gopal,¹ R. Suresh,^{1, a)} and V. K. Chandrasekar^{1, b)}

Department of Physics, Centre for Nonlinear Science and Engineering, School of Electrical and Electronics Engineering, SASTRA Deemed University, Thanjavur 613 401, India

(Dated: 4 May 2021)

The amplitude-dependent frequency of the oscillations, termed *nonisochronicity*, is one of the essential characteristics of nonlinear oscillators. In this paper, the dynamics of the Rössler oscillator in the presence of nonisochronicity is examined. In particular, we explore the appearance of a new fixed point and the emergence of a coexisting limit-cycle and quasiperiodic attractors. We also describe the sequence of bifurcations leading to synchronized, desynchronized attractors and oscillation death states in the coupled Rössler oscillators as a function of the strength of nonisochronicity and coupling parameters. Further, we characterize the multistability of the coexisting attractors by plotting the basins of attraction. Our results open up the possibilities of understanding the emergence of coexisting attractors, and into a qualitative change of the collective states in coupled nonlinear oscillators in the presence of nonisochronicity.

Nonisochronicity is one of the essential and peculiar characteristic property of the nonlinear differential equations. We show here that for Rössler oscillator with nonisochronicity term, there exist many distinct dynamical states, due to the appearance of a new fixed point, which leads to rich and complex dynamics in the system. We observe that the coexistence of many attractors may introduce additional sensitivity and randomness in the chaotic system because an infinitesimal perturbation in initial values is sufficient for a trajectory to shift from one state to another. This can be of great interest for secure communication applications through encryption of information-based chaos, for example, and various control strategies in engineering contexts. We describe and characterize the regions of synchronization in coupled Rössler oscillators, basins of attraction corresponding to different attractors using master stability function formalism. We also observe that the system's permutational symmetry is broken at a critical value of the coupling strength, which persuades multi-stable synchronized, desynchronized attractors, and oscillation death states in the coupled Rössler oscillators.

I. INTRODUCTION

Systems that are described by the nonlinear differential equations are omnipresent ranging from biological systems to physical systems and economics¹⁻³. The nonlinearities present in these systems facilitate the emergence of rich dynamical states such as self-sustained oscillations, turbulence, and chaos, which are impossible to obtain in the systems described by the linear differential equations. In particular, one of the important characteristics of nonlinear differential equations is the amplitude-dependent frequency of nonlinear oscillations, known as nonisochronicity, the term first used in

ref.⁴. Nonisochronicity is central to inhomogeneities that can be seen in a variety of living situations^{5,6} and due to this nonisochronous nature of the nonlinear equations, different responses have been observed for different input conditions in practical or experimental settings. In particular, when considering the complex biological or other networks, the strong nonisochronicity often results in rich synchronization patterns and the level of isochronicity of oscillators is an important property of the phase interaction function, where the strong dependence of the oscillatory period or frequency on the amplitude results in high-level shear in the phase dynamics and coupling can dramatically change the oscillatory period⁷. Also, it has been reported that the higher nonisochronicity level can induce long, irregular transient phase dynamics in the networks, where such long transient dynamics have relevance in the functioning of biological systems⁸. The detection of isochrons in a system is also prescribed recently^{9,10}. Moreover, nonisochronicity plays a significant role in the development of anomalous phase synchronization in populations of nonidentical oscillators¹¹, which has also been experimentally confirmed^{12,13}. Further, in the networks of nonlocally coupled Stuart-Landau oscillators, the nonisochronicity leads to the emergence of various collective states such as amplitude chimera, amplitude cluster, frequency chimera, frequency cluster states, imperfect and mixed imperfect synchronized states, local and global chimera states, etc., which have been recently reported in the case of symmetry preserving and symmetry breaking couplings¹⁴⁻¹⁸. Similarly, the emergence of nonisochronicity induced chimera, and chimera-like states in nonlocally and globally coupled complex Ginzburg-Landau model¹⁹⁻²¹, van der Pol system²² are also demonstrated. Furthermore, in ref.²³, the authors reported that the nonisochronicity could also be used to control the transition to synchronization in an ensemble of nonidentical oscillators.

As mentioned earlier, the strong nonisochronicity parameter induces rich collective dynamics in a coupled system of oscillators. However, the role of nonisochronicity has been mainly studied in the case of Stuart-Landau oscillator, coupled complex Ginzburg-Landau model and only a few studies are reported in other dynamical systems. Nevertheless, there are many other interesting nonlinear oscillatory systems and

^{a)}Electronic mail: sureshphy.logo@gmail.com.

^{b)}Electronic mail: chandru25nld@gmail.com.

biological models that deserve to be studied in detail in the presence of nonisochronicity. In compliance with this, in a recent study²⁴, the authors have reported the advent of chimera states due to the presence of nonisochronicity term in a diffusively coupled global network of Rössler oscillators. They also found that the presence of multistability^{25–32} is the key mechanism for the appearance of coexisting states. Moreover, the emergence of chimera state in a star network of Rössler oscillators with nonisochronicity term is demonstrated with various coupling topologies³³.

Further, in Ref.³⁴, the authors have explored the possibility of controlling chaos in an ensemble of modified Rössler oscillators, in which the individual nodes are indirectly coupled through a single external oscillator. Furthermore, the investigation of the emergence of chaotic phase synchronization in three coupled modified Rössler oscillator systems with parameter mismatches are reported³⁵. The authors showed the switching between complete and partial phase synchronization as a function of the coupling strength. The transition from in-phase to out-of-phase synchronizations via the phase-flip transition in a network of relay-coupled modified Rössler oscillators is demonstrated by Sharma et al.³⁶. In all the studies mentioned above, the Rössler oscillator with nonisochronicity term has been used to demonstrate the results. However, the basic knowledge of the dynamical changes that occurred in the Rössler oscillator with nonisochronicity parameter is still lagging. Additionally, the study of nonisochronicity term induced bifurcations and collective dynamical states exhibited in the coupled systems with different coupling topologies are required exhaustive investigation.

Taking this as our motivation, in this paper, we study the dynamics of the Rössler oscillator by adding the nonisochronicity term. Without which the system exhibits limit-cycle oscillations for the chosen parameter values. When we incorporate the nonisochronicity term into the oscillator equation, the system manifests the coexistence of limit-cycle and quasiperiodic attractors. This is due to the appearance of a new fixed point in response to the strength of the nonisochronicity parameter. Next, the study is extended to a system of two mutually coupled Rössler oscillators, and we investigate the influence of the coupling parameter along with the nonisochronicity term. We show that when one increases the strength of coupling, by fixing the nonisochronicity parameter, the permutational symmetry $((x_1, y_1, z_1) \leftrightarrow (x_2, y_2, z_2))$ of the subsystems is broken at a critical value of the coupling strength, that persuades multistable desynchronized attractors, which are emerged via different bifurcations based on the strength of nonisochronicity and coupling parameters.

When the coupling strength reaches a sufficiently larger value, the symmetry is preserved again, which leads one of the attractors to exhibit synchronized oscillations. Here, the synchronization is defined as the correlation of both phase and amplitude of the oscillations. During the occurrence of desynchronized oscillations, either amplitude or both phase and amplitude are uncorrelated. In addition to the synchronized and desynchronized oscillations, we discover the development of two distinct oscillation death (OD) states (in which the subsystems exhibit inhomogeneous steady-state so-

lutions) along with the synchronized and desynchronized oscillations. The occurrence of steady state solutions^{37–44} and multistability^{30–32} has been reported in networks of original Rössler oscillators with different coupling configurations. However, we emphasize that to the best of our knowledge, the emergence of OD states and coexisting attractors are unexplored yet in the coupled Rössler oscillators with nonisochronicity term. Further, the multistability is characterized by estimating the bifurcation diagrams, and the region of complete synchronization is identified using the master stability function (MSF) formalism. Also, based on the emergence of different attractors, the bifurcation plot is divided into several regions. The development of coexisting attractors in those regions is corroborated by plotting the basins of attraction.

The structure of the remaining paper is organized as follows: In Sec. II, we will introduce the mathematical model of the Rössler oscillator with nonisochronicity term, and discuss the stability of the fixed points of the system with and without the nonisochronicity term. In Sec. III, we study the dynamics of a Rössler oscillator with nonisochronicity term and show the emergence of coexisting attractors that are emerged via various bifurcations. Next, in Sec. IV, we will consider two mutually coupled oscillators for our study and show the emergence of coexisting synchronized, desynchronized attractors along with OD states using bifurcation diagrams. Further, the bifurcation diagram is divided into different regions based on the combination of coexisting attractors, and the multistability is confirmed by plotting the basins of attraction in Sec. V. Moreover, the probability of occurrence of each attractor in the basins is also discussed. Finally, the obtained results are consolidated, and the future directions of research are discussed in Sec. VI.

II. MATHEMATICAL MODEL AND FIXED POINT ANALYSIS

In order to demonstrate our results, we first consider a Rössler oscillator with nonisochronicity term, which can be described by the mathematical equation of the form

$$\begin{aligned}\dot{x} &= -\omega_0(1 - \alpha(x^2 + y^2))y - z, \\ \dot{y} &= \omega_0(1 - \alpha(x^2 + y^2))x + ay, \\ \dot{z} &= b + (x - c)z,\end{aligned}\tag{1}$$

where x, y , and z are the state variables, ω_0 is the natural frequency of the system, a, b , and c are the control parameters. α is a parameter to adjust the strength of nonisochronicity.

In order to find the fixed points, the three Rössler equations are set to zero and the resulting equations of x and z -components can be written in terms of the y -variable as follows,

$$\begin{aligned}x &= \frac{acy^2}{ay^2 + b}, \quad z = \frac{ay^2 + b}{c}, \\ f(y)_\alpha &= cy\omega_0 \left(1 - \alpha \left(\frac{a^2c^2y^4}{(ay^2 + b)^2} + y^2 \right) \right) + ay^2 + b = 0.\end{aligned}\tag{2}$$

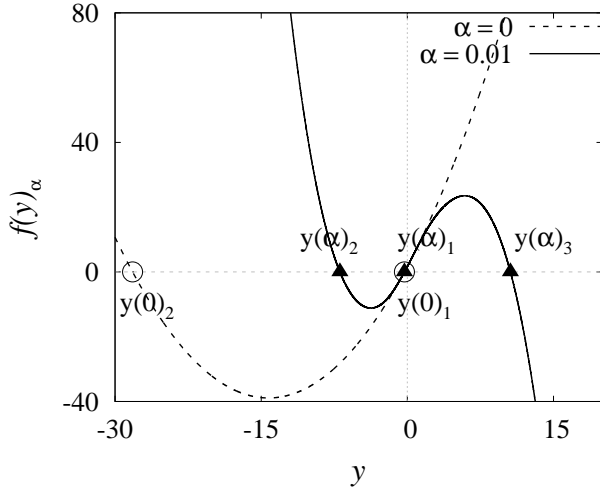


FIG. 1. Fixed points of the y -component of a Rössler oscillator (1) in the absence of nonisochronicity parameter ($\alpha = 0$) and for $\alpha = 0.01$. The system parameters are fixed at $\omega_0 = 1$, $a = 0.2$, $b = 1.7$ and $c = 5.7$.

For $\alpha = 0$, the function $f(y)_\alpha$ in Eq. (2) becomes

$$f(y)_0 = y(ay + c\omega_0) + b, \quad (3)$$

and the corresponding two roots (fixed points) are given by

$$y(0)_{1,2} = \pm \frac{\sqrt{c^2\omega_0^2 - 4ab}}{2a} - c\omega_0. \quad (4)$$

The respective two fixed points $y(0)_1$ and $y(0)_2$ are depicted as open circles in Fig. 1 for the fixed values of the control parameters $\omega_0 = 1$, $a = 0.2$, $b = 1.7$ and $c = 5.7$. When $\alpha \neq 0$, the function $f(y)_\alpha$ has three roots (fixed points) $y(\alpha)_{1,2,3}$. The fixed points $y(\alpha)_{1,2}$ are the same fixed points that were present when $\alpha = 0$, however the positions are now dependent on the value of α (see filled triangles in Fig. 1). They are approximately given by the following form

$$y(\alpha)_{(1,2)} \approx \left(a^2\beta^5 (5a\beta - 2c\omega_0(2\alpha c^2 + 3\alpha\beta^2 - 2)) + b^2\beta^2(3a - 2\alpha c\omega_0\beta) + ab\beta^3(9a\beta + 4c\omega_0(1 - 2\alpha\beta^2)) - b^3 \right) \times \left(6a^3\beta^5 + a^2\beta^3(12b + c\omega_0(-5\alpha c^2 - 7\alpha\beta^2 + 5)) + 2ab\beta \left(3b + c\omega_0\beta(3 - 5\alpha\beta^2) \right) + b^2c\omega_0(1 - 3\alpha\beta^2) \right)^{-1} \quad (5)$$

where $\beta = y(0)_{(1,2)}$. To find the fixed points of Eq. (1), the nonisochronicity parameter α is considered as a small perturbation. The other fixed point $y(\alpha)_3$ is newly emerged upon introducing α . This can be clearly seen from Fig. 1 that the new fixed point has emerged in the positive y -direction due to the effect of α . For the aforementioned values of control parameters, the three fixed points are unstable and the nature of their eigenvalues are

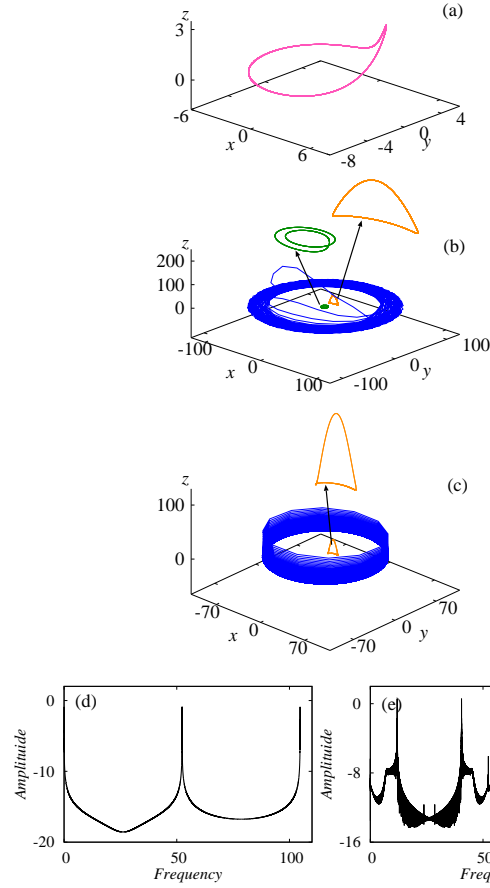


FIG. 2. The attractors that are emerged for different values of the nonisochronicity parameter (α) in the Rössler oscillator (1). Other parameters are fixed as shown in Fig. 1. (a) Three dimensional projection of the period-I limit-cycle attractor emerged for $\alpha = 0$, (b) shows the period-II attractor along with the coexisting period-I attractor and large-amplitude quasiperiodic attractor for different sets of initial states, for $\alpha = 0.007$, (c) depicts the coexistence of period-I limit-cycle and quasiperiodic attractors that are appeared in the system for $\alpha = 0.01$. (d) and (e) Depicts the power spectrum of the periodic and quasiperiodic attractors (shown in Fig.2(c)), respectively.

1. $FP(\alpha)_1 = (x(\alpha)_1, y(\alpha)_1, z(\alpha)_1)$ – which has one negative real eigenvalue (near zero) and one complex conjugate eigenvalue pair with a positive real part.
2. $FP(\alpha)_2 = (x(\alpha)_2, y(\alpha)_2, z(\alpha)_2)$ – which has one complex conjugate eigenvalue pair with a negative real part and one positive real eigenvalue.
3. $FP(\alpha)_3 = (x(\alpha)_3, y(\alpha)_3, z(\alpha)_3)$ – which has one negative real eigenvalue and one complex conjugate eigenvalue pair with a positive real part.

When $\alpha = 0$, the system shows a single limit-cycle attractor, for the above chosen parameter values, which is rotating about the fixed point $y(0)_1$. When introducing α , due to the emergent of a new fixed point $y(\alpha)_3$, the system shows additional limit-cycle and quasiperiodic attractors. We explain

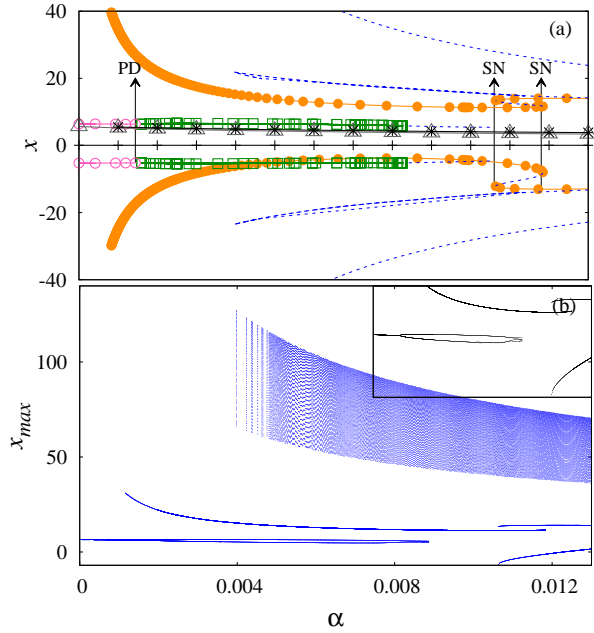


FIG. 3. (a), (b) Bifurcation diagrams of a single Rössler oscillator model (1) as a function of the nonisochronicity parameter $\alpha \in [0, 0.013]$, shows the emergence of different dynamical states. The evolution of three fixed points are depicted as lines with open triangle, asterisk, and plus symbol. Other system parameters are fixed as given in Fig. 1.

this in detail in Sec. III. One can also notice that in the case of $c^2 \omega_0^2 < 4ab$, the system (1) has zero (one) fixed point for $\alpha = 0$ ($\neq 0$).

III. DYNAMICS OF AN INDIVIDUAL RÖSSLER OSCILLATOR WITH NONISOCHRONICITY

First, we study the dynamics of Eq. (1) as a function of the nonisochronicity parameter (α). For our numerical investigation, we have integrated Eq. (1) using the fourth-order Runge-Kutta method with a step size of 0.01. We also confirm that the similar results can be observed when we use smaller time-steps of 0.001. The emerging attractors are depicted in Fig. 2 for three selective values of α . First, in the absence of α , as mentioned earlier, the Rössler oscillator has two fixed points ($FP(0)_1$ and $FP(0)_2$), in that $FP(0)_2$ is saddle-focus whose one-dimensional unstable manifold repels the trajectories along the stable manifold of the other fixed point $FP(0)_1$, which is also a saddle-focus. Therefore, a period-I limit-cycle attractor is emerged, which rotates (counter-clockwise) around $FP(0)_1$ fixed point. The three-dimensional projection of the respective limit-cycle attractor in the (x, y, z) phase plane is displayed in Fig. 2(a) for $\alpha = 0$. When we incorporate and slowly increase the nonisochronicity parameter further, the period-I limit-cycle is then bifurcated into a period-II attractor via period-doubling bifurcation. At the same time, due to the inclusion of α , one more new fixed point $FP(\alpha)_3$ has emerged in the system, as shown in Fig. 1. Consequently, an

other period-I limit-cycle appears for different sets of initial states, which rotate around the fixed point $FP(\alpha)_3$. In addition to this, a large-amplitude quasiperiodic attractor is also appeared and rotating around the fixed points $FP(\alpha)_1$, $FP(\alpha)_2$ and $FP(\alpha)_3$. All three coexisting attractors that are emerged for different sets of initial states are depicted in Fig. 2(b) for the value of $\alpha = 0.007$. The periodic (period-I attractor) and quasiperiodic nature of the attractors are confirmed by estimating the power spectrum and are plotted in Figs. 2(d), and 2(e), respectively. The period-II attractor has become unstable when α reaches a threshold value. Therefore, only the other two attractors are stable and coexisted in the system, which is depicted in Fig. 2(c) for $\alpha = 0.01$.

Overall, the Rössler oscillator (1) exhibits coexisting limit-cycle and quasiperiodic attractors when we incorporate the nonisochronicity parameter in it. To acquire a clear picture of the dynamics of the system, the bifurcation diagram of Eq (1) is depicted in Fig. 3(a) as a function of $\alpha \in [0, 0.013]$, which is obtained using the XPPAUT software package⁴⁵. In this figure, the lines with different points represent various stable attractors, and the broken lines indicate the unstable periodic orbits. In particular, the lines with open circles in Fig. 3(a) indicate the maxima and minima of the period-I limit-cycle oscillations equivalent to the attractor shown in Fig. 2(a). The period-doubling bifurcation, which occurred at the critical value of $\alpha = 0.0016$, is marked as PD in Fig. 3(a). The lines with open squares indicate the maxima and minima of the respective period-II attractor, and this period-II orbit is then become unstable when $\alpha > 0.0082$. The newly emerged period-I limit-cycle attractor for other sets of initial conditions is coexisted along with the period-II orbit is also depicted in Fig. 3(a) as lines with solid circles. The labels SN indicates the saddle-node bifurcation. The evolution of the three fixed points (lines with open triangle, asterisk, and plus symbols) with respect to α is also depicted in Fig. 3(a). Among them the newly emerged fixed point is depicted with asterisk symbol.

The emergence of multistable attractors for different set of initial conditions as a function of the nonisochronicity parameter can be confirmed again in Fig. 3(b), in which the maxima of the system variable x (x_{max}) are plotted as a function of α , shows the qualitative changes that occurred in the system. The bifurcation of the periodic orbits and the emergence of quasiperiodic states can be clearly visualized in Fig. 3(b) with respect to α . The inset in Fig. 3(b) elucidate the period-doubling phenomenon.

Further, to identify the initial states to which different attractors emerge in the system, the basins of attraction of the Rössler oscillator is plotted in Figs. 4(a) and 4(b) by fixing $z = -1$ for $\alpha = 0.007$ and 0.01, respectively (corresponding to the attractors depicted in Figs. 2(b) and 2(c)). In Fig. 4(a), the green (dark gray) colored region indicates the basin of attraction of the period-II limit-cycle attractor, the area of orange (light gray) color represents the basin of attraction of the period-I limit-cycle attractor, and finally, the blue (black) color domain portrays the initial states to which the large-amplitude quasiperiodic attractor emerge in the system. We wish to emphasize here that, for our upcoming study,

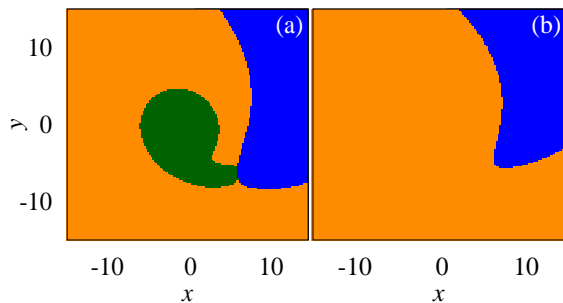


FIG. 4. Basins of attraction of the system (1) as a function of the system variables x and y for (a) $\alpha = 0.007$, and (b) $\alpha = 0.01$ shows the emergence of coexisting attractors for different initial states.

we choose the initial states only from the limit-cycle region and omit the initial states, which leads to the large-amplitude quasiperiodic oscillations.

Thus, an individual Rössler oscillator exhibits coexisting attractors with respect to the strength of the nonisochronicity parameter. It is also of interest to investigate the dynamics of the coupled system and how the coupling parameter, along with the nonisochronicity term, influence the system dynamics. Therefore, in Sec. IV, we will consider two mutually coupled system of Rössler oscillators and study the dynamics as a function of the coupling and nonisochronicity parameters.

IV. DYNAMICS OF THE COUPLED RÖSSLER OSCILLATOR AND THE INFLUENCE OF NONISOCHRONICITY AND COUPLING PARAMETERS

The mathematical model of a system of two mutually coupled Rössler oscillators can be given as

$$\begin{aligned}\dot{x}_{1,2} &= -\omega_0(1 - \alpha(x^2 + y^2))y_{1,2} - z_{1,2} + \varepsilon(x_{2,1} - x_{1,2}), \\ \dot{y}_{1,2} &= \omega_0(1 - \alpha(x^2 + y^2))x_{1,2} + ay_{1,2}, \\ \dot{z}_{1,2} &= b + (x_{1,2} - c)z_{1,2},\end{aligned}\quad (6)$$

where ε (≥ 0) represents the strength of diffusive coupling. In Eq. (6), if we vary the coupling strength, by fixing α as a constant, the coupled system undergoes critical bifurcations. Consequently, different desynchronized attractors have emerged due to the breaking of the system's permutational symmetry and coexisted for different sets of initial states, including the birth of two different OD states. The one-parameter bifurcation diagram is estimated as a function of ε by fixing α to display the development of different bifurcations and show the transition to complete synchronization state of the coupled system.

The bifurcation diagram of the coupled system (6) is depicted in Fig. 5 for $\varepsilon \in [0, 2.5]$, and $\alpha = 0.01$. Again, the stable orbits are identified using the lines with different points, and broken lines indicate the unstable orbits. The vertical dashed lines represent the critical values of ε , at which different bifurcations occur. Also, they separate the bifurcation diagram into different regions based on the bifurcations that

occur. In the absence of coupling, both subsystems exhibit the coexistence of period-I limit-cycle and large-amplitude quasiperiodic attractors, as depicted in Fig. 2(c). In particular, the period-I limit-cycles of the subsystems oscillate with equal amplitude, satisfying the permutational symmetry $(x_1, y_1, z_1) \leftrightarrow (x_2, y_2, z_2)$, but the phases are uncorrelated (exhibit constant phase shift), characterized as homogeneous oscillations-1 and the attractors are named as H_1 . The solid diamonds in Fig. 5 for $\varepsilon = 0$ represent the maxima and minima of the homogeneous oscillations. When we slowly increase the coupling strength beyond $\varepsilon > 0.001$, three different attractors have newly emerged in the system and coexisted for different initial states. These three attractors are further brought to the number of attractors as a function of the coupling strength, via different bifurcation routes. To be more specific, the systems exhibit desynchronized period-I limit-cycle attractor (H_2) along with two different quasiperiodic attractors, namely QP_1 and QP_2 . The quasiperiodic dynamics is confirmed again by estimating the power spectrum. In the following, how these three attractors bifurcated and give birth to new attractors via different bifurcations as a function of ε is explained.

1. In the attractor H_2 , both the subsystems begin to evolve with different amplitudes (due to the breaking of permutational symmetry), but still rotating with the common center of rotation, which is called as homogeneous oscillations-2. The line with open circles in Fig. 5 indicates the maxima and minima of the attractor H_2 . The time series and related phase space plots of the desynchronized attractor H_2 are depicted in Figs. 6(c) and 6(d), respectively, for $\varepsilon = 0.14$. The attractor H_2 is stable until $\varepsilon = 2.356$ and when we increase the coupling strength to $\varepsilon > 2.356$, the attractor H_2 attains the complete synchronization manifold, and the symmetry is again preserved in the subsystems. The emerged synchronized attractor is labeled as S (lines with inverted triangles in Fig. 5), and the time series as well as the phase portrait plots of the attractor S are depicted in Figs. 6(e) and 6(f), respectively, for $\varepsilon = 3.0$.
2. Secondly, the QP_1 has emerged in the system, if we choose the initial states from another basin of attraction. The two attractors are rotating around the different centers of rotation. We named this attractor as QP_1 , and this quasiperiodic attractor is stable in the range of the coupling strength $\varepsilon \in (0.001, 0.147]$. The time evolution and the phase space plots of the QP_1 attractor are plotted in Figs. 7(a) and 7(b) for $\varepsilon = 0.14$. When we increase the coupling strength further, the QP_1 attractor lost its stability through torus bifurcation (marked as TB_1 in Fig. 5) and transformed into stable desynchronized limit-cycle oscillations for $\varepsilon > 0.147$. The lines with crosses indicate the maxima and minima of the corresponding limit-cycle attractor. Here, both the oscillators have a different center of rotation, which is shown in Figs. 7(c) and 7(d) for $\varepsilon = 0.25$. We named these attractors as IH_1 (inhomogeneous oscillations-1). The amplitude of the attractor IH_1 is slowly decreases-

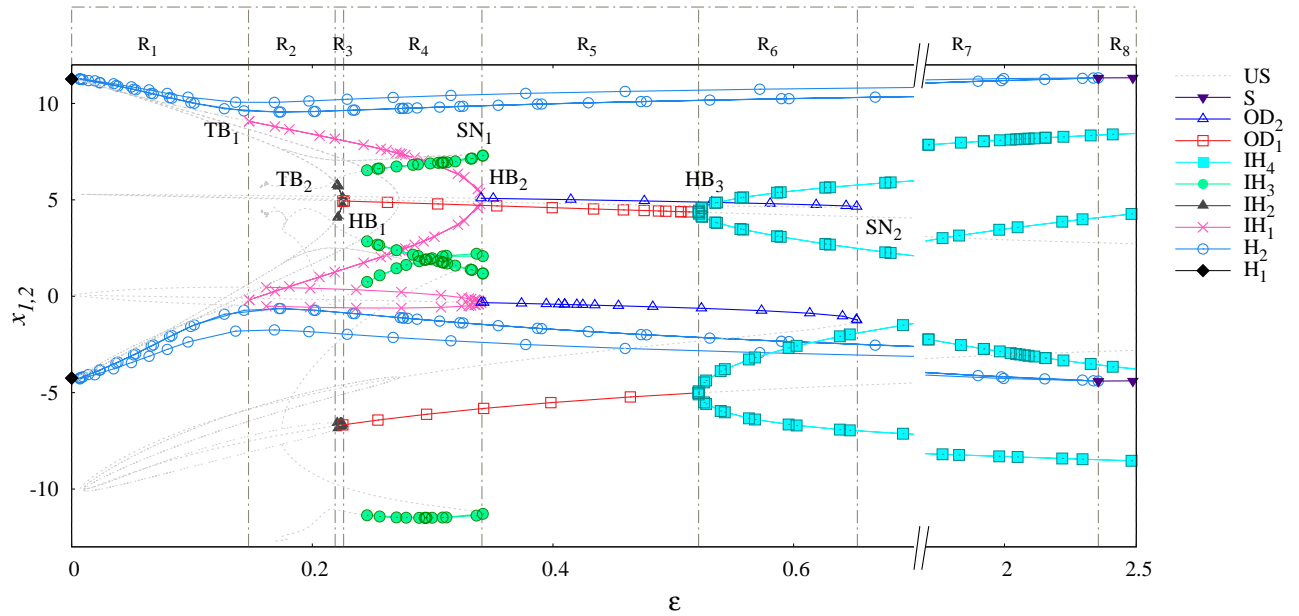


FIG. 5. Bifurcation diagram of the system (6) illustrates the occurrence of different bifurcations and multiple attractors as a function of the coupling strength $\varepsilon \in [0, 2.5]$ for $\alpha = 0.01$. The vertical dashed lines indicate the critical values of ε , in which different bifurcations occur and separates the region from R_1 to R_8 . Other parameters are fixed as given in Fig. 1.

TABLE I. Table shows the emergence of different attractors in system(6) as a function of coupling strength $\varepsilon \in [0, 2.5]$ for nonisochronicity parameter $\alpha = 0.01$.

Attractor name	Oscillation type	Range of $\varepsilon \in [0, 2.5]$
H_1	Homogeneous oscillations-1	$0 < \varepsilon \leq 0.001$
QP_1	Quasiperiodic oscillations-1	$0.001 < \varepsilon \leq 0.147$
QP_2	Quasiperiodic oscillations-2	$0.001 < \varepsilon \leq 0.22$
H_2	Homogeneous oscillations-2	$0.001 < \varepsilon \leq 2.356$
IH_1	Inhomogeneous oscillations-1	$0.147 < \varepsilon \leq 0.34$
IH_2	Inhomogeneous oscillations-2	$0.22 < \varepsilon \leq 0.225$
OD_1	Oscillation death state-1	$0.225 < \varepsilon \leq 0.521$
IH_3	Inhomogeneous oscillations-3	$0.245 < \varepsilon \leq 0.341$
OD_2	Oscillation death state-2	$0.341 < \varepsilon \leq 0.653$
IH_4	Inhomogeneous oscillations-4	$\varepsilon > 0.521$
S	Synchronized oscillations	$\varepsilon > 2.356$

ing when one increases the coupling strength, and for $\varepsilon = 0.341$, the attractor IH_1 is transformed into OD state-2 (attractor OD_2) that has emerged via reverse supercritical Hopf bifurcation. The lines with open triangles in Fig. 5 represent attractor OD_2 , and the critical coupling strength of the Hopf bifurcation point is labeled as HB_2 in Fig. 5. This steady-state is portrayed in Figs. 7(e) and 7(f) for $\varepsilon = 0.4$. Upon increasing the coupling strength further, the OD state-2 and another unstable fixed point collides with each other and disappeared via saddle-node bifurcation when the coupling strength reaches the value of $\varepsilon = 0.653$. The respective bifurcation point is marked as SN_2 in Fig. 5.

3. Finally, QP_2 attractor exhibits in the range of $\varepsilon \in (0.001, 0.22]$. The QP_2 attractor also rotates about the

different center of rotations. The time series and phase space plots of the QP_2 attractor are depicted in Figs. 8(a) and 8(b), respectively, for $\varepsilon = 0.14$ indicating that the amplitude of the QP_2 attractor is relatively smaller than QP_1 . Next, if we increase ε further, the QP_2 attractor is then bifurcated into stable limit-cycle attractor through torus bifurcation (TB_2) at $\varepsilon = 0.22$ (see Fig. 5). The newly emerged limit-cycles also have two different centers of rotation and oscillate with different amplitudes corroborated from the time evolution and phase portraits, as depicted in Figs. 8(c) and 8(d), respectively, for $\varepsilon = 0.221$. We named this attractor as IH_2 (inhomogeneous oscillations-2). These limit-cycles are stable only for a short range of ε (filled triangles in Fig. 5) and then bifurcated into an OD state-1 (OD_1)

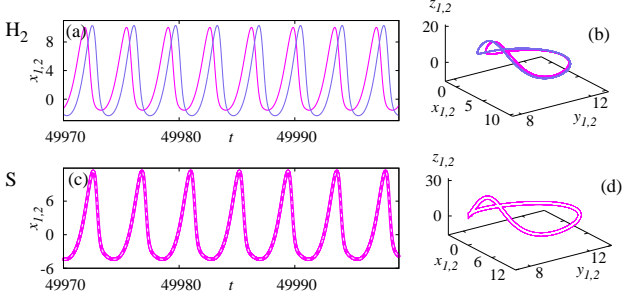


FIG. 6. Time evolution and the corresponding phase portraits of the system (6) obtained for different initial states for $\alpha = 0.01$. [(a), (b)] Homogeneous oscillations–2 (H_2) for $\varepsilon = 0.14$, and [(c), (d)] shows the synchronized oscillations (S) of the subsystems for $\varepsilon = 3.0$.

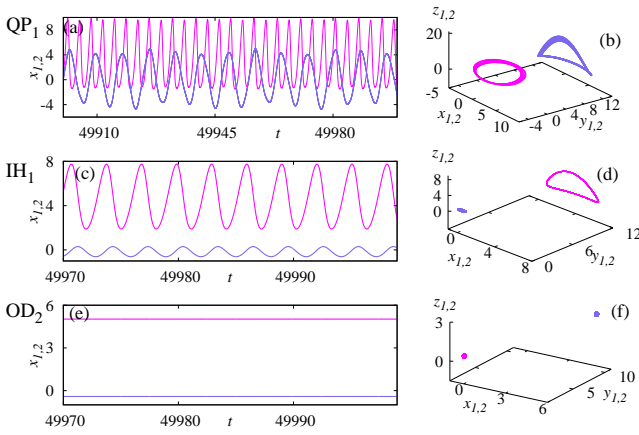


FIG. 7. Time evolution and the respective phase portraits of the system (6) obtained for $\alpha = 0.01$. [(a), (b)] Quasiperiodic oscillations–1 (QP_1) obtained for another set of initial states for $\varepsilon = 0.14$, [(c), (d)] inhomogeneous oscillations–1 (IH_1) for $\varepsilon = 0.25$, and [(e), (f)] shows the OD state–2 (OD_2) for $\varepsilon = 0.4$.

for $\varepsilon = 0.225$ via reverse supercritical Hopf bifurcation, at which the two systems attain different stable, steady-states. For instance, the corresponding states are portrayed in Figs. 8(e) and 8(f) for $\varepsilon = 0.25$. The critical Hopf bifurcation point is marked as HB_1 in Fig. 5 and the open squares depicted the attractor OD_1 . After that, the OD_1 attractor is lost stability and transformed into a stable limit-cycle attractor (denoted by the solid squares in Fig. 5) for $\varepsilon = 0.521$ via supercritical Hopf bifurcation. The newly emerged attractor also have two different origins of rotation, which are named as IH_4 (inhomogeneous oscillations–4). The associated time series and phase portraits of the IH_4 attractor are depicted in Figs. 8(g) and 8(h), respectively, for $\varepsilon = 0.8$ confirming that the amplitudes are uncorrelated (desynchronized). Finally, only two limit-cycle attractors IH_4 (desynchronized) and S (synchronized) are stable and coexisted.

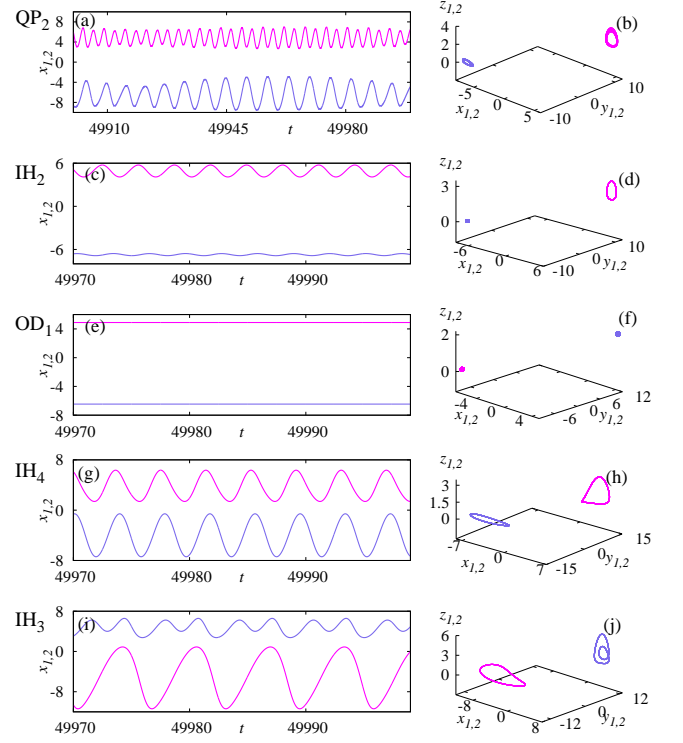


FIG. 8. Time evolution and the equivalent phase portraits of the system (6) obtained for different initial states for $\alpha = 0.01$. [(a), (b)] Quasiperiodic oscillations–2 (QP_2) for $\varepsilon = 0.14$, [(c), (d)] inhomogeneous oscillations–2 (IH_2) for $\varepsilon = 0.221$, [(e), (f)] OD state–1 (OD_1) obtained for an another set of initial states for $\varepsilon = 0.25$, [(g), (h)] inhomogeneous oscillations–4 (IH_4) for $\varepsilon = 0.8$, and [(i), (j)] shows the emergence of inhomogeneous oscillations–3 (IH_3) for $\varepsilon = 0.25$.

Meanwhile, when the coupling strength reaches the value of $\varepsilon = 0.245$, an unstable periodic orbit is bifurcated into a stable limit-cycle which is indicated as inhomogeneous oscillations–3 and the corresponding attractors are named as IH_3 (solid circles in Fig. 5), in which one of the subsystems oscillate with period-II limit-cycle oscillations, and the other subsystem exhibits period-I limit-cycle oscillations which are evident from Figs. 8(i) and 8(j), plotted for $\varepsilon = 0.25$. These attractors are stable until the coupling strength reaches the value of $\varepsilon = 0.341$. After that, the attractor IH_3 is merged with an unstable orbit and disappeared via saddle-node bifurcation (denoted as SN_1 in Fig. 5).

Thus, the influence of coupling, along with nonisochronicity parameters, is studied in terms of the bifurcation diagram. The emergence of different bifurcations, and coexisting synchronized and desynchronized attractors are discussed. In a nutshell, Table I shows the possible attractors that are appeared in the system (6) as a function of $\varepsilon \in [0, 2.5]$ for $\alpha = 0.01$. Next, based on the emergence of different coexisting attractors, the bifurcation diagram is divided into a number of regions, and basins of attraction of each region are described in Sec. V.

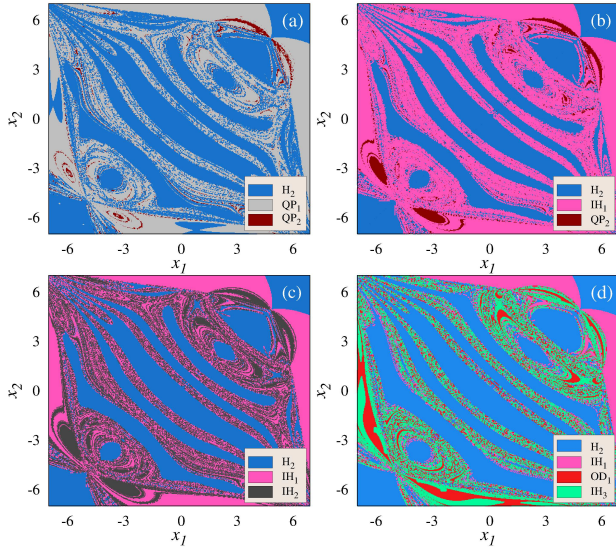


FIG. 9. Basins of attraction of the system (6) as a function of the state variables x_1 and x_2 for different values of the coupling strength ϵ with $\alpha=0.01$, (a) plotted for $\epsilon=0.1$, (b) for $\epsilon = 0.18$, (c) for $\epsilon = 0.221$ and (d) is depicted for $\epsilon = 0.25$. The inset shows the riddled nature of the basin in certain ranges of initial states.

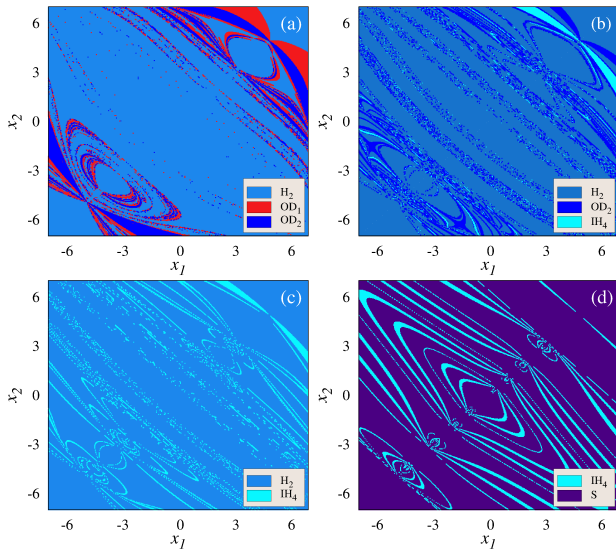


FIG. 10. Basins of attraction of the system (6) as a function of the state variables x_1 and x_2 for different values of the coupling strength ϵ with $\alpha=0.01$, (a) plotted for $\epsilon=0.4$, (b) for $\epsilon = 0.6$, (c) for $\epsilon = 0.8$ and (d) is depicted for $\epsilon = 3.0$.

V. BASINS OF ATTRACTION IN DIFFERENT REGIONS OF THE BIFURCATION DIAGRAM

Based on the appearance of different bifurcations, Fig. 5 is divided into eight regions from R_1 to R_8 , in which different coexisting attractors have emerged for different initial states as a function of the coupling strength. In the following, we

discuss the basins of attraction of those regions. It is important to emphasize here that in order to plot the basins of attraction of the coupled system, the initial states of the x -variables of the two individual systems are uniformly distributed in the range of $x_{1,2} \in [-7, 7]$ and the initial states of the other state variables are fixed at $y_{1,2} = 0.5$ and $z_{1,2} = -1$.

In region R_1 , the system exhibits the coexistence of attractors H_2 , QP_1 , and QP_2 . The basins of attraction of the respective attractors are depicted in Fig. 9(a) for $\epsilon = 0.1$. In this figure, the blue (dark gray) color region represents the basin of attraction of attractor H_2 . The light gray color region indicates the basin of attraction of the QP_1 , and the initial states to which the attractor QP_2 has emerged are indicated by the region of maroon (black) color. We can also note that the attractors H_2 and QP_1 are having an almost equal number of occurrences. The attractor QP_2 has occurred for less number of initial states than the other two attractors. Next, in region R_2 of the bifurcation diagram, the coupled system exhibits the coexistence of attractors H_2 , IH_1 , and QP_2 , in which IH_1 has occurred relatively for a large number of initial states than the other two attractors. The corresponding basins of attraction are plotted in Fig. 9(b) for $\epsilon = 0.18$, where at the pink (light gray) color portrays the basin of attraction of IH_1 attractor. Next, the attractors H_2 , IH_1 and IH_2 coexist in the region R_3 for different sets of initial states and the respective basins of attraction is plotted in Fig. 9(c) for the value of coupling strength $\epsilon = 0.221$. The dark gray color points illustrate the initial states to which the IH_2 has emerged in the system, and IH_1 dominates the other two attractors with a high number of occurrences. Further, the system (6) shows the coexistence of four different attractors including H_2 , IH_1 , OD_1 , and IH_3 in region R_4 . The basins of attraction of those attractors are depicted in Fig. 9(d) for the value of coupling strength $\epsilon = 0.25$ corroborating that H_2 has a high number of occurrences. The red (dark gray) color indicates the basin of attraction of OD_1 , and the light green (gray) color illustrates the basin of attraction of the attractor IH_3 .

Moreover, in region R_5 , the coupled system exhibits the coexistence of two OD states (OD_1 and OD_2) with attractor H_2 . For instance, the corresponding basins of attraction is plotted in Fig. 10(a) for $\epsilon = 0.4$ in which the dark blue (black) color region describes the basin of attraction of the attractor OD_2 . Next, the basins of attraction in the region R_6 are plotted in Fig. 10(b) for $\epsilon = 0.6$ in that the system shows the coexistence of the attractors H_2 , OD_2 , and IH_4 . The aqua (light gray) color indicates the basin of attraction of IH_4 . Furthermore, the basins of attraction of region R_7 is depicted in Fig. 10(c) for $\epsilon = 0.8$ at which only the attractors $A1$ and IH_4 are co-occurred. In all these Figs. 10(a), 10(b) and 10(c) the attractor H_2 dominates the other attractors with a high number of occurrences. Finally, in region R_8 , the newly emerged synchronized attractor S has coexisted with IH_4 , and dominates the basin of attraction with a high number of occurrences, which is plotted for $\epsilon = 3.0$ in Fig. 10(d).

Therefore, from Figs. 9 and 10, one can observe that each attractor dominates the other attractors with a high number of occurrences for large values of initial states. Therefore it is also of interest to investigate the probability of different attrac-

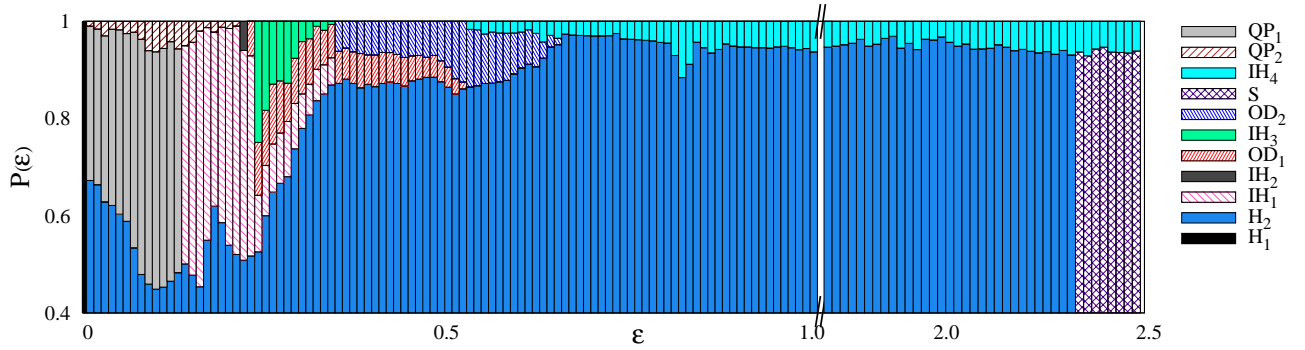


FIG. 11. Probability of various attractors from H_1 to S including the quasiperiodic attractor QP_1 and QP_2 as a function of the coupling strength and for $\alpha = 0.01$. Different colors and patterns indicate the probability of different attractors.

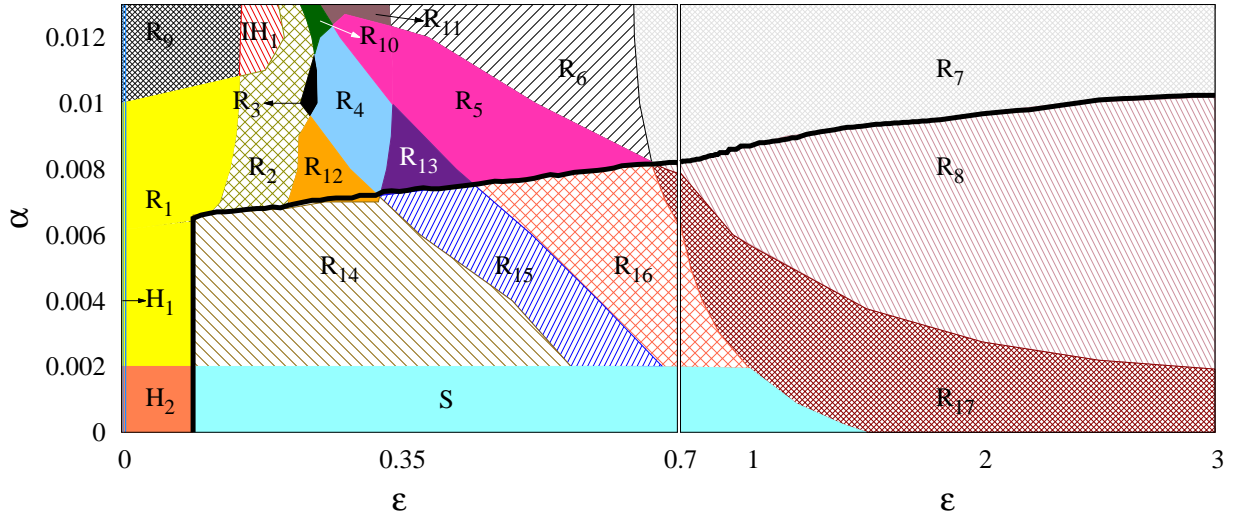


FIG. 12. Emergence of multistable attractors for different initial states are illustrated in a two-parameter diagram of the coupled Rössler oscillator (6) as a function of nonisochronicity parameter ($\alpha \in [0, 0.013]$) and coupling strength $\varepsilon \in [0, 3]$. Distinct colors and patterns represent the combination of different attractors. The combination of attractors in regions R_1 to R_8 are already illustrated in Sec. V. The combination of attractors in other regions from R_9 to R_{17} are as follows: R_9 indicates the coexistence of attractors H_2 and QP_1 . Similarly, $R_{10} = H_2 + IH_1 + OD_1 + IH_3$, $R_{11} = H_2 + IH_3 + OD_2 + IH_4$, $R_{12} = H_2 + IH_1 + IH_3$, $R_{13} = H_2 + IH_1 + OD_1$, $R_{14} = IH_1 + S$, $R_{15} = IH_1 + OD_1 + S$, $R_{16} = OD_1 + OD_2 + S$, $R_{17} = OD_2 + IH_4 + S$. The thick black continuous line indicates the complete synchronization region obtained using MSF formalism (8). The parameter values are fixed as given in Fig. 1

tors with respect to the coupling parameter ε^{46-48} . Figure 11 shows the probability of various attractors for 500 uniformly distributed initial states of $x_{1,2} \in [-7, 7]$ for $\alpha = 0.01$ and as a function of ε . From Fig. 11, one can easily uncover that the attractor H_1 predominantly occurs in the probability diagram with a high number of occurrences and shares the basin of attraction with other coexisting attractors for $\varepsilon < 2.356$. After that, the S attractor dominates the basin to our calculated range of $\varepsilon = 3.0$ and shares the parameter space with IH_4 .

To clarify the coexistence of different attractors, we have plotted a two-phase diagram in the parameter space of $\varepsilon \in [0, 3]$ and $\alpha \in [0, 0.013]$ in Fig. 12, which depicts the multistability of attractors for different values of ε and α . Each colored and patterned regions indicate the coexistence of different attractors. One can also notice that, apart from the regions

R_1 to R_8 as discussed earlier, there exist other combinations of coexisting attractors in regions from R_9 to R_{17} which are also indicated in Fig. 12. For an illustration, in region R_{15} , the attractors IH_1 , OD_1 and S coexist and the respective basins of attraction is plotted in Fig. 13(a) for $\varepsilon = 0.5$ and $\alpha = 0.006$. Similarly, the basins of attraction of the region R_{16} is plotted in Fig. 13(b) for $\varepsilon = 0.6$ and $\alpha = 0.006$, in which OD_1 and OD_2 are coexisting along with the synchronized attractor S .

The region of the stable synchronized state for the coupled system (6) is identified using the well-known MSF formalism. The complete synchronization manifold is defined by $x_1 = x_2 = x$, $y_1 = y_2 = y$ and $z_1 = z_2 = z$, where x, y, z are the solutions of the uncoupled system (1). Let, (η_j, ξ_j, ζ_j) are the deviations of (x_j, y_j, z_j) , $j = 1, 2$ from the synchronized solu-

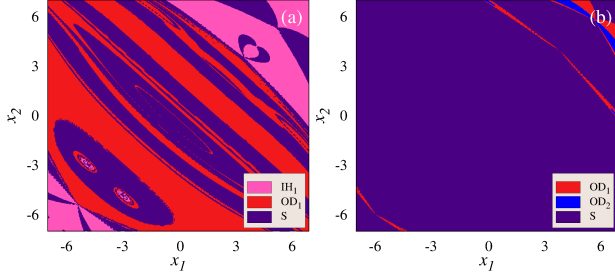


FIG. 13. The basins of attraction of the coupled Rössler oscillator (6) for (a) $\varepsilon = 0.5$, and (b) for $\varepsilon = 0.6$ with $\alpha = 0.006$ shows the coexisting attractors in the regions of R_{15} and R_{16} , respectively.

tion (x, y, z) and we have

$$\begin{aligned}\dot{\eta}_{1,2} &= -\omega_0(\xi_{1,2} - \alpha(2xy\eta_{1,2} + (x^2 + 3y^2)\xi_{1,2})) - \zeta_{1,2} + \varepsilon(\eta_{2,1} - \eta_{1,2}) \\ \dot{\xi}_{1,2} &= \omega_0(\eta_{1,2} - \alpha(2yx\xi_{1,2} + (3x^2 + y^2)\eta_{1,2})) + a\xi_{1,2} \\ \dot{\zeta}_{1,2} &= x\xi_{1,2} + z\eta_{1,2} - c\zeta_{1,2}.\end{aligned}\quad (7)$$

From Eq. (7) we get,

$$\begin{aligned}\dot{\eta} &= -\omega_0(\xi - \alpha(2xy\eta + (x^2 + 3y^2)\xi)) - \zeta - 2\varepsilon\eta \\ \dot{\xi} &= \omega_0(\eta - \alpha(2yx\xi + (3x^2 + y^2)\eta)) + a\xi \\ \dot{\zeta} &= x\xi + z\eta - c\zeta,\end{aligned}\quad (8)$$

where $(\eta, \xi, \zeta) = (\eta_1 - \eta_2, \xi_1 - \xi_2, \zeta_1 - \zeta_2)$ are the transverse small perturbations on the synchronization manifolds. The synchronized state is stable when all the transverse perturbations (η, ξ, ζ) tend to zero when $t \rightarrow \infty$. This will happen when all the transverse Lyapunov exponents are negative. Using the equation (8) we have identified the region of stable complete synchronization state in (ε, α) parameter space. The thick black continuous line in Fig. 12 represents the region of stable complete synchronization.

VI. CONCLUSIONS

In summary, we have systematically studied the influence of nonisochronicity on the single and mutually coupled Rössler oscillator. First, we have examined the fixed point analysis of a single Rössler oscillator with and without nonisochronicity term. We showed that adding the nonisochronicity term can increase the number of fixed points, which induces multistability of coexisting limit-cycle and quasiperiodic attractors. Next, we have extended our studies to a system of two mutually coupled Rössler oscillators and investigated the influence of the coupling parameter along with the nonisochronicity parameter. We showed that the permutational symmetry of the coupled system is broken when one increases the coupling strength, persuades multistability of desynchronized attractors, which are emerged via different bifurcations. The broken symmetry is preserved again in the system when the coupling strength reaches higher values, engenders the emergence of a synchronized attractor. In addition

to the synchronized and desynchronized attractors, we have reported the emergence of two different OD states. The results are corroborated using the bifurcation diagrams, and basins of attraction. The region of complete synchronization is identified using the MSF formalism.

The results presented in the paper are robust against system parameters, and similar results can be observed even if the systems exhibit chaotic dynamics. Also, we note that the results are obtained only in the two coupled systems. However, it is also of interest to understand the interplay of nonisochronous nature of the system and coupling topology in different network architectures to induce rich collective dynamical behaviors and to identify the network topologies that enhance or support the effects of nonisochronicity are still open problems, and we are processing our research in this direction.

ACKNOWLEDGMENTS

C. Ramya acknowledges SASTRA for financial support in the form of Teaching Assistantship. The work of R. S. is supported by the SERB-DST Fast Track scheme for young scientists under Grant No. YSS/2015/001645. The work of V. K. C. and R. G. are sponsored by the SERB-DST-CRG Grant No. CRG/2020/004353 and CSIR EMR Grant No. 03(1444)/18/EMR-II. All the authors thank DST, New Delhi for computational facilities under the DST-FIST programme (SR/FST/PS-1/2020/135) to the Department of Physics.

DATA AVAILABILITY

The data that support the findings of this study are available from the corresponding author upon reasonable request.

- ¹S. Strogatz, *Nonlinear Dynamics and chaos: with applications to physics, biology, chemistry, and engineering*, (CRC Press, London 2018).
- ²A. W. Leung, *Systems of nonlinear partial differential equations: applications to biology and engineering*, (Springer, Netherlands 1989).
- ³T. Puu, *Attractors, Bifurcations and Chaos: Nonlinear Phenomena in Economics*, (Springer-Verlag, Berlin 2003).
- ⁴D. G. Aronson, G. B. Ermentrout, N. Kopell, "Amplitude response of coupled oscillators," *Physica D* **41**, 403 (1990).
- ⁵H. Daido, K. Nakanishi, "Diffusion-induced inhomogeneity in globally coupled oscillators: swing-by mechanism," *Phys. Rev. Lett.* **96**, 054101 (2006).
- ⁶V. S. Tiberkevich, R. S. Khymyn, H. X. Tang, A. N. Slavin, "Sensitivity to external signals and synchronization properties of a non-isochronous auto-oscillator with delayed feedback," *Sci. Rep.* **4**, 3873 (2014).
- ⁷M. Sebek, R. Tönjes, I. Z. Kiss, "Complex rotating waves and long transients in a ring-network of electrochemical oscillators with sparse random cross-connections," *Phys. Rev. Lett.* **116**, 068701 (2016).
- ⁸M. Wickramasinghe, I. Z. Kiss, "Synchronization of electrochemical oscillators with differential coupling," *Phys. Rev. E* **88**, 062911 (2013).
- ⁹A. Mauroy and I. Mezić, "On the use of Fourier averages to compute the global isochrons of (quasi)periodic dynamics," *Chaos* **22**, 033112 (2012).
- ¹⁰A. Mauroy and I. Mezić, J. Moehls "Isostables, isochrons, and Koopman spectrum for the action-angle representation of stable fixed point dynamics," *Physica D* **261**, 19 (2013).
- ¹¹B. Blasius, E. Montbrió, J. Kurths, "Anomalous phase synchronization in populations of nonidentical oscillators," *Phys. Rev. E* **67**, 035204(R) (2003).
- ¹²S. K. Dana, B. Blasius, J. Kurths, "Experimental evidence of anomalous phase synchronization in two diffusively coupled Chua oscillators," *Chaos* **16**, 023111 (2006).

- ¹³M. Wickramasinghe, E. M. Mrugacz, I. Z. Kiss, "Dynamics of electrochemical oscillators with electrode size disparity: asymmetrical coupling and anomalous phase synchronization," *Phys. Chem. Chem. Phys.* **13**, 15483 (2011).
- ¹⁴K. Premalatha, V. K. Chandrasekar, M. Senthilvelan, M. Lakshmanan, "Impact of symmetry breaking in networks of globally coupled oscillators," *Phys. Rev. E* **91**, 052915 (2015).
- ¹⁵K. Premalatha, V. K. Chandrasekar, M. Senthilvelan, M. Lakshmanan, "Imperfectly synchronized states and chimera states in two interacting populations of nonlocally coupled Stuart-Landau oscillators," *Phys. Rev. E* **94**, 012311 (2016).
- ¹⁶K. Premalatha, V. K. Chandrasekar, M. Senthilvelan, M. Lakshmanan, "Different kinds of chimera death states in nonlocally coupled oscillators," *Phys. Rev. E* **93**, 052213 (2016).
- ¹⁷K. Premalatha, V. K. Chandrasekar, M. Senthilvelan, M. Lakshmanan, "Stable amplitude chimera states in a network of locally coupled Stuart-Landau oscillators," *Chaos* **28**, 033110 (2018).
- ¹⁸D. V. Senthilkumar, V. K. Chandrasekar, "Coexistence of Coherence and incoherence in nonlocally coupled phase oscillators," *Nonlin. Phen. Complex Syst.* **5**, 380 (2002).
- ¹⁹Y. Kuramoto, D. Battogtokh, "Local and global chimera states in a four-oscillator system," *Phys. Rev. E* **100**, 032211 (2019).
- ²⁰G. Sethia, A. Sen, "Chimera States: The Existence Criteria Revisited," *Phys. Rev. Lett.* **112**, 144101 (2014).
- ²¹A. Mishra, C. Hens, M. Bose, P. K. Roy, S. K. Dana, "Chimeralike states in a network of oscillators under attractive and repulsive global coupling," *Phys. Rev. E* **92**, 062920 (2015).
- ²²C. R. Hens, A. Mishra, P. K. Roy, A. Sen, S. K. Dana, "Chimera states in a population of identical oscillators under planar cross-coupling," *Pramana J. Phys.* **84**, 229 (2015).
- ²³E. Montbrió, B. Blasius, "Using nonisochronicity to control synchronization in ensembles of nonidentical oscillators," *Chaos* **13**, 291 (2003).
- ²⁴V. K. Chandrasekar, R. Gopal, A. Venkatesan, M. Lakshmanan, "Mechanism for intensity induced chimera states in globally coupled oscillators," *Phys. Rev. E* **90**, 062913 (2014).
- ²⁵J. C. Sommerer, E. Ott, "A physical system with qualitatively uncertain dynamics," *Nature* **365**, 138 (1993).
- ²⁶U. Feudel, C. Grebogi, L. Poon, J. A. Yorke, "Dynamical properties of a simple mechanical system with a large number of coexisting periodic attractors," *Chaos Soliton Fract.* **9**, 171 (1998).
- ²⁷Y. Do, Y.-C. Lai, "Multistability and arithmetically period-adding bifurcations in piecewise smooth dynamical systems," *Chaos* **18**, 043107 (2008).
- ²⁸Y.-C. Lai, C. Grebogi, "Quasiperiodicity and suppression of multistability in nonlinear dynamical systems," *Eur. Phys. J. Special Topics* **226**, 1703 (2017).
- ²⁹T. T. Wontchui, J. Y. Effa, H. P. E. Fouda, S. R. Ujjwal, R. Ramaswamy, "Coupled Lorenz oscillators near the Hopf boundary: Multistability, intermingled basins, and quasiriddling," *Phys. Rev. E* **96**, 062203 (2017).
- ³⁰Hens, H. R., Banerjee, R., Feudel, U., Dana, S. K.: How to obtain extreme multistability in coupled dynamical systems. *Phys. Rev. E* **85**, 035202(R) (2012).
- ³¹P. Jaros, P. Perlikowski, T. Kapitaniak, "Synchronization and multistability in the ring of modified Rössler oscillators," *Eur. Phys. J. Special Topics* **224**, 1541 (2015).
- ³²M. S. Patel, U. Patel, A. Sen, G. C. Sethia, C. Hens, S. K. Dana, U. Feudel, K. Showalter, C. N. Ngonghala, R. E. Amritkar, "Experimental observation of extreme multistability in an electronic system of two coupled Rössler oscillators," *Phys. Rev. E* **89**, 022918 (2014).
- ³³C. Meena, K. Murali, S. Sinha, "Chimera states in star networks," *Int. J. Bifurc. Chaos Appl. Sci. Eng.* **26**, 1630023 (2016).
- ³⁴S. S. Chaurasia, S. Sinha, "Suppression of chaos through coupling to an external chaotic system," *Nonlinear Dyn.* **87**, 159–167 (2017).
- ³⁵I. Nishikawa, N. Tsukamoto, K. Aihara, "Switching phenomenon induced by breakdown of chaotic phase synchronization," *Physica D* **238**, 1197–1202 (2009).
- ³⁶A. Sharma, M. D. Shrimali, A. Prasad, R. Ramaswamy, and U. Feudel, "Phase-flip transition in relay-coupled nonlinear oscillators," *Phys. Rev. E* **84**, 016226 (2011).
- ³⁷A. Prasad, "Amplitude death in coupled chaotic oscillators," *Phys. Rev. E* **72**, 056204 (2005).
- ³⁸G. Saxena, A. Prasad, and R. Ramaswamy, "Amplitude death: The emergence of stationarity in coupled nonlinear systems," *Phys. Rep.* **521**, 205 (2012).
- ³⁹V. Resmi, G. Ambika, R. E. Amritkar, "General mechanism for amplitude death in coupled systems. *Phys. Rev. E* **84**, 046212 (2011).
- ⁴⁰V. Resmi, G. Ambika, R. E. Amritkar, and G. Rangarajan, "Amplitude death in complex networks induced by environment," *Phys. Rev. E* **85**, 046211 (2012).
- ⁴¹C. R. Hens, O. I. Olusola, P. Pal, and S. K. Dana, "Oscillation death in diffusively coupled oscillators by local repulsive link," *Phys. Rev. E* **88**, 034902 (2013).
- ⁴²M. Nandan, C. R. Hens, P. Pal, and S. K. Dana, "Transition from amplitude to oscillation death in a network of oscillators," *Chaos* **24**, 043103 (2014).
- ⁴³U. K. Verma, A. Sharma, N. K. Kamal, and M. D. Shrimali, "First order transition to oscillation death through an environment," *Phys. Lett. A* **382**, 2122–2126 (2018).
- ⁴⁴U. K. Verma, A. Sharma, N. K. Kamal, and M. D. Shrimali, "Explosive death in complex network," *Chaos* **29**, 063127 (2019).
- ⁴⁵B. Ermentrout, "Simulating, Analyzing and Animating Dynamical System: A Guide to Xppaut for Researchers and Students," pp.161-169 . SIAM, Philadelphia (2002).
- ⁴⁶P. J. Menck, J. Heitzig, N. Marwan, and J. Kurths "How basin stability complements the linear-stability paradigm," *Nat. Phys.* **9**, 89 (2013).
- ⁴⁷P. Schultz, P. J. Menck, J. Heitzig, and J. Kurths "Potentials and limits to basin stability estimation," *New J. Phys.* **19**, 023005 (2017).
- ⁴⁸P. Brzeski and P. Perlikowski, "Sample-based methods of analysis for multistable dynamical systems," *Arch. Comput. Methods Eng.* **26**, 1515 (2019).